Ostwald ripening of three-dimensional clusters on a surface studied with an ultrafast kinetic Monte Carlo algorithm

Geoffroy Prévot

Institut des NanoSciences de Paris, Université Paris 6 – UMR CNRS 7588 4, place Jussieu, FR-75252 Paris cedex 05, France

(Received 21 March 2011; revised manuscript received 1 June 2011; published 18 July 2011)

We have studied the Ostwald ripening of three-dimensional islands on a homogeneous surface with an original off-lattice kinetic Monte Carlo algorithm. In this algorithm, adatom trajectories are highly simplified, while still ensuring that the adatom fluxes between islands are exactly described. From the simulations, we obtained the evolution of the island size distribution over a large time range. The simulations obtained are compared with the results of numerical integration of rate equations derived from a mean-field approximation. Both results indicate that the equilibrium radius of the islands follows a power-law behavior in the limit of a very dilute phase, with an exponent close to 1/4. A general, excellent agreement is obtained, showing the validity of our approach, whereas the validity of the mean-field approximation is discussed for a very small mean island size, or for a large fraction of the surface covered by the islands.

DOI: 10.1103/PhysRevB.84.045434 PACS number(s): 68.55.A−, 81.15.Aa

I. INTRODUCTION

The dynamics of phase separation on a surface is a key parameter for numerous technological processes such as thin-film growth or aging of catalysts.[1] For example, starting from a continuous film deposited onto a substrate, annealing can lead to dewetting, formation of particles of the deposited species on top of the substrate surface, and coarsening of the particle assembly. Two main processes can be involved in the coarsening of a particle assembly: particle migration followed by coalescence, and capillarity-driven interparticle transport, known as Ostwald ripening. In this process, diffusing species detach from the particles, diffuse onto the substrate, and condense on other particles. Due to their higher chemical potential, small clusters shrink at the expense of larger ones. Since the seminal works of Lifshitz, Slyosov, and Wagner (LSW)[2,3] for three-dimensional clusters in bulk (3D/3D), various studies have been devoted to Ostwald ripening of particles, including also monolayer islands on a surface (2D/2D) and three-dimensional islands on a surface (3D/2D).

Two regimes are usually distinguished: the diffusion-limited[2] and attachment-limited[3] regimes. In the first case, there is no extra barrier for attachment of atoms to the island periphery (for simplicity, we will take atoms as an example of diffusing species in the whole paper). Atoms attach to an island as soon as they reach its perimeter. As a result, there is no discontinuity of the chemical potential at the interface between the island and the bare surface, and the chemical potential of the atoms varies continuously between the particles. In the second case, due to the extra barrier for attachment, the chemical potential is not continuous at the interface between the island and the surface, but is nearly constant between the particles. Note that for both cases, the kinetics of coarsening is first of all limited by the detachment of the atoms from the particles.

In the past, two main predictions have been obtained from the LSW 3D/3D analytical model: first, the critical radius, i.e., the radius of a cluster in temporary equilibrium with the concentration of adatoms, follows a power-law growth rate. For the diffusion-limited coarsening, the rate exponent is equal to 1/3, and for the attachment-limited coarsening, it is equal to 1/2. Secondly, the asymptotic cluster-size distribution $n(R,t)$ has a self-similar behavior.

The LSW model has also been extended to ripening of islands on surfaces. Analytical solutions were first given by Chakraverty for 3D/2D,[4] with a growth exponent of 1/4 for diffusion-limited coarsening, and a rate exponent of 1/3 for attachment-limited coarsening. The theoretical results obtained (size distribution and rate exponent) were often used as a criterion for discriminating between attachment-limited coarsening and diffusion-limited coarsening. For example, for Sn/Si(111) (Ref. 5) and Sn/Si(100) (Ref. 6) coarsening kinetics, a growth exponent of 1/4 was extracted from the late stage of coarsening, whereas the evolution was slower for the early stage of coarsening, leading to the conclusion that Ostwald ripening was limited by diffusion. On the contrary, a 1/3 growth exponent has been found for Pd/alumina[7] and a 1/2 growth exponent has been observed for coerced mechanical coarsening induced by the tip of an atomic force microscope on a particle assembly.[8]

More sophisticated descriptions have been developed in order to take into account the effects of faceting,[9,10] nonuniform interfacial energy,[11] quantum size effects,[12] interfacial stress,[13] or mixing.[14] Few works have questioned the validity of the LSW approach for islands on a surface. Contrary to the 3D/3D case, the mean-field approach of the LSW developed is *a priori* not valid for two-dimensional (2D) diffusion due to the absence of a steady-state solution of the diffusion equation for an isolated circular source on an infinite surface. In the model of Chakraverty, an arbitrary cut-off length is introduced in order to suppress the logarithmic divergence of the diffusion field. This cut-off length should be related to the distance between islands and reflects the fact that islands are not isolated. A more sophisticated model has been given by Marqusee[15] in order to correctly treat the influence of the nearest neighbors on the growth rate of a given particle. Using an "effective medium" approach, he self-consistently derived a growth law and asymptotic distribution for the 2D/2D diffusion-limited case. The rate exponent was found to be 1/3, with a prefactor depending on the area fraction, and the distribution could be obtained numerically. This power law

was confirmed by kinetic Monte Carlo simulations,[16] whereas the effects of faceting were shown to markedly modify the growth exponent.[17]

The approach of Marqusee has also been extended to 3D/2D diffusion-limited systems by Shorlin *et al.*[18] They showed that in the limit of a very dilute phase, i.e., when the islands cover a negligible area fraction, the growth law for the critical radius could be approximated with a 1/4 power law modified with a logarithmic correction. However, due to the very large experimental uncertainties and to the lack of efficient simulation algorithms, the 3D/2D analytical predictions could hardly be verified up to now.

Two methods have been used for simulating the kinetics of 3D/2D Ostwald ripening: either by solving the diffusion equations for an initial configuration of islands, or by performing kinetic Monte Carlo (KMC) simulations. The direct resolution of Fick equations[19] has been mainly employed for analyzing the evolutions of epitaxial quantum dots where stress also plays a role.[20,21] However, the simulations are generally limited to a few particles. Full 3D on-lattice KMC algorithms have been used for simulation of growth,[22–26] in the frame of the "solid on solid" model, with energy barriers usually derived from the bond-counting scheme. The effects of annealing have been studied on a flat film that undergoes dewetting upon annealing,[25] but only the initial stages were accessible. In order to increase the computation speed, coarse-grained KMC algorithms with 2D on-lattice diffusion have been developed for the study of growth[27] and coarsening.[28] In these algorithms, islands are described as hemispheres evolving only by exchange of atoms through diffusion on the substrate lattice and the detachment rate of atoms from the islands is treated in a mean-field approximation. The gain in CPU is most important at the beginning of the simulation when interisland spacing is small. When the mean distance between islands increases, the computation speed decreases. At the same time, multiscale[29] or first-passage algorithms[30] have been developed to speed up the computation of diffusion processes. We have combined these two approaches and developed a new KMC algorithm, for studies of Ostwald ripening, which considerably increases the computation speed.

In this paper, we present a comparison between the analytical mean-field theory of Marqusee and Shorlin *et al.* (MS) and the results of this ultrafast coarse-grained Monte Carlo algorithm. The first part is devoted to the presentation of the analytical model. The Monte Carlo algorithm is described in detail in the second part, whereas the last part is devoted to the presentation of the numerical results and their comparison with the analytical results.

II. ANALYTICAL MEAN-FIELD MODEL

The derivation of a mean-field analytical solution for the 2D/2D and 3D/2D cases is well described in the works of Marqusee[15] and Shorlin *et al.*[18] Briefly, let us recall the main results. In this part, we consider a population of 3D islands on a solid homogeneous flat surface. We assume that the island surface free energy γ is isotropic.

Islands have, at thermal equilibrium, the shape of a spherical cap, i.e., a portion of a sphere of radius R_S. θ is the corresponding contact angle with the substrate. In the following, we will consider that θ is independent of R_S, even if for small islands, line tension effects can lead to a variation of θ with R_S.[31,32] The footprint of the islands onto the substrate is a disk of radius $R_D = R_S \sin(\theta)$. Of course, for crystalline islands, γ depends on the surface orientation and the cluster shape can more or less deviate from the sphere cap shape, depending on the temperature.

Each island is considered to be in an effective medium at a mean concentration $\bar{c}$. The flux $J_T(R_D)$ into an island of radius R_D is proportional, within a so-defined factor $k(R_D)$, to the difference between $\bar{c}$ and the equilibrium concentration at the island periphery $c_{eq}(R_S)$.

$$J_T(R_D) = k(R_D)[\bar{c} - c_{eq}(R_S)]. \tag{1}$$

$c_{eq}(R_S)$ is given by the Gibbs-Thomson relationship

$$c_{eq}(R_S) = c_{eq}(R_S = \infty) \exp\left(\frac{2\gamma\Omega}{kTR_s}\right), \tag{2}$$

where Ω is the atomic volume and $c_{eq}(R_S = \infty)$ is the equilibrium concentration for an island of infinite size. $k(R_D)$ is *a priori* unknown and depends on the distribution of island radius $n(R_D)$ at the surface.

The mean concentration $\bar{c}$ evolves as

$$\frac{\partial \bar{c}(t)}{\partial t} = \int_0^\infty k(R_D,t)n(R_D,t)[c_{eq}(R_S) - \bar{c}(t)]\, dR_D. \tag{3}$$

The equilibrium radius $\bar{R}_D$ is defined as the radius of an island at equilibrium in a homogeneous concentration field $c(\vec{r}) = \bar{c}$. $\bar{R}_D$ is thus simply given by $c_{eq}[\bar{R}_D/\sin(\theta)] = \bar{c}$. The local concentration field $c(\vec{r})$ obeys a modified equation of diffusion, given by

$$\frac{\partial c(\vec{r},t)}{\partial t} = D\nabla^2 c(\vec{r},t) - D\xi^{-2}c(\vec{r},t) + S, \tag{4}$$

where

$$D\xi^{-2} = \int_0^\infty k(R_D,t)n(R_D,t)dR_D \tag{5}$$

is the sink term for the concentration field and

$$S = \int_0^\infty k(R_D,t)n(R_D,t)c_{eq}(R_S)dR_D \tag{6}$$

is the source term. ξ plays the role of a screening length and removes the divergence present in the single particle case. During the coarsening, the adatom concentration rapidly reaches an equilibrium state which slowly evolves conversely with the evolution of $n(R_D)$.

At the time scale of adatom diffusion, $\partial c(\vec{r},t)/\partial t = 0$ and the source and sink term balance for the mean concentration: $D\xi^{-2}\bar{c} = S$. Writing $\delta c(\vec{r}) = c(\vec{r}) - \bar{c}$, Eq. (4) simplifies to

$$(\nabla^2 - \xi^{-2})\delta c(\vec{r}) = 0. \tag{7}$$

The solution of Eq. (7) is[15]

$$c(r) = \bar{c} + \frac{K_0(r/\xi)}{K_0(R_D/\xi)}[c_{eq}(R_S) - \bar{c}], \tag{8}$$

where K_0 is the zeroth modified Bessel function of the second kind.

The local flux into the island is given by

$$J_T = 2\pi R_D D \frac{\partial c}{\partial r}(R_D) = \frac{2\pi R_D D}{\xi} \frac{K_1(R_D/\xi)}{K_0(R_D/\xi)}[\bar{c} - c_{eq}(R_S)], \tag{9}$$

where K_1 is the first modified Bessel function of the second kind.

The number of atoms in an island is given by

$$N = \frac{4}{3}\frac{\pi\alpha(\theta)}{\Omega} R_D^3, \tag{10}$$

where $\alpha(\theta) = [2 - 3\cos(\theta) + \cos^3(\theta)]/[4\sin^3(\theta)]$.

Since $J_T = dN/dt$, the evolution of island radius becomes

$$\frac{\partial R_D}{\partial t} = \frac{\Omega D}{2R_D\xi\alpha(\theta)} \frac{K_1(R_D/\xi)}{K_0(R_D/\xi)}[\bar{c} - c_{eq}(R_S)]. \tag{11}$$

Using Eqs. (2) and (9), a self-consistent equation for ξ can then be obtained:

$$\xi^{-1} = 2\pi \int_0^\infty R_D n(R_D) \frac{K_1(R_D/\xi)}{K_0(R_D/\xi)} dR_D. \tag{12}$$

The evolution of the system is thus entirely given by Eq. (11), Eq (12), and the mass conservation equation

$$\frac{4}{3}\frac{\pi\alpha(\theta)}{\Omega}\frac{\partial}{\partial t}\int_0^\infty n(R_D)R_D^3 dR_D + \frac{\partial \bar{c}}{\partial t} = 0. \tag{13}$$

The second term in Eq. (13) can be rapidly neglected since practically all atoms are in the islands.

Due to the presence of Bessel functions in Eq. (11), the system of equations (11)–(13) does not follow any power-law evolution. However, in the limit of very low island density, i.e., for $R_D << \xi$, it has been demonstrated[18] that the equilibrium radius should be proportional to $t^{1/4}$.

For the comparison with KMC simulations, we have performed a numerical integration of Eq. (11) using different initial configurations and the value of ξ computed, at each integration step, through the self-consistent equation (12). For each island size, the growth rate is calculated with Eq. (11), using a value of $\bar{c}$ that ensures that the mass is conserved. Islands disappear as soon as their size is below the atomic radius. In that case, the sizes of the remaining islands are recomputed in order to maintain a constant total mass.

III. KINETIC MONTE CARLO ALGORITHM

KMC is a very useful method for simulating the evolution of systems out of equilibrium or for measuring the fluctuations of systems at thermal equilibrium, providing that the relevant activated processes are known. Accordingly, KMC simulations have been successfully used to model a variety of dynamical processes ranging from thin-film growth to catalysis.

Kinetic Monte Carlo simulations for growth and coarsening of particles on surfaces are usually based on the Bortz, Kalos, and Lebowitz (BKL) algorithm.[33] In this algorithm, each elemental move of the system is associated with a frequency given by an Arrhenius law. For each step, a basic move is selected according to its frequency and the time evolves as the inverse of the sum of all frequencies of the possible moves. Most of the KMC developed for growth and coarsening use a lattice for the definition of the atomic positions, which leads to a few basic moves. A basic change is usually the motion of an atom from one site to a neighboring site, but more complicated changes—including the concerted motion of many atoms—can be added.[16,34,35] It is, however, often difficult to calculate all the possible atomic-scale events that may be important in a simulation, and so KMC simulations have a relatively limited rate catalog. The selection of the basic move is made on the database of possible events which usually correspond to a wide range of frequencies. These frequencies can be determined by using the bond-counting scheme: the difference between the number of bonds before and after the atomic jump determines the energy barrier to overlap for the motion, and the frequency follows a corresponding Arrhenius law with an attempt frequency in the $10^{12} - 10^{13}$Hz range. *Ab initio* simulations can also be used for the determination of the energy barriers on systems with a restricted number of atoms. In both cases, the energy barriers are much lower for the diffusion of an atom on the substrate or at the surface of the particle than for the detachment of an atom from a particle. In a full 3D KMC in a solid-on-solid frame, most of the CPU time is used for diffusion of atoms at the border of the particle. If this can be interesting for the study of island motion and reshaping, it is much too CPU consuming for the study of coarsening.

In order to avoid these problems, coarse-grained KMC algorithms have been recently developed for the study of Ostwald ripening.[28] In these algorithms, islands have an ideal shape and interact only through their footprint on the substrate. They evolve by exchange of atoms through diffusion on the substrate lattice sites. The detachment rate of atoms from the islands is treated in a mean-field approximation. For large distances between islands, most of the CPU time is spent in the computation of the atomic diffusion on the substrate. Moreover, as soon as the interparticle distance becomes large with respect to the particle in-plane radius, atoms that leave a given particle have a probability close to unity to reattach to the same particle. This is due to the fact that for a 2D random walk, the probability of return to the origin is equal to unity. The system is thus quenched in a quasistable state evolving slowly due to the very rare events which are the diffusion of atoms from one island to another. In the original off-lattice KMC algorithm presented here, the atomic diffusion is treated separately from the detachment of adatoms from the islands, with a coarse-grained treatment of the atomic trajectory.

In the simulation, we consider 3D islands on an atomically flat homogeneous surface with periodic boundary conditions applied. Islands are considered to be isotropic, unstrained, and locally at equilibrium, i.e., their shape is governed by the free-surface energies of the islands γ_p and of the substrate γ_s, and by the interface free energy γ_{ps}. The effect of island reshaping has been discussed by Shorlin *et al.*,[18] for the case where the detachment and attachment rates are high enough to induce a shape variation of the particle with growth rate. Only particles having their radius close to the equilibrium radius adopt an equilibrium shape. In the following, we have always assumed that island reshaping occurs at a much higher frequency than detachment or attachment. Particles thus have a truncated spherical shape, with a contact angle θ given by $\gamma_p \cos(\theta) = \gamma_s - \gamma_{ps}$. In the surface plane, the footprint of the particles is thus a disk of size $R_D = R_S \sin(\theta)$. We also

neglect the variation of γ_p with R_S.[36] Atomistic simulations using Lennard-Jones potentials have shown that γ_p behaves as $\gamma_p(R) = \gamma_p(\infty)/[(1 + 2(l_S/R_S)^2]$ with a characteristic length l_S close to the interatomic distance.[37] This leads to a greater than 10 % variation of the surface energy for particles of radius less than 1 nm. Such effects have been observed for Pb/MgO.[38]

For islands of few atoms, magic size effects leading to a nonmonotonic variation of surface energy with size can dominate.[39] We neglect all these effects, which are specific to each situation, in order to focus on the first-order size effects on the chemical potential.

In the simulation, atoms detach from particles, diffuse, and attach to other particles. We use the BKL algorithm for definition of the time scale: at each step, the probabilities of all events are summed, which defines the time step. A random number is then generated and used for choosing a possible move according to its probability. The table of events is organized in a binary tree. In a standard KMC algorithm, the possible events listed are the detachment, the diffusion, or the attachment of atoms. In order to increase the computation speed, we have proceeded in a very different way than standard KMC algorithms. In the present simulation, during a single time step, an atom detaches from an island, diffuses onto the substrate, and attaches to another island. Thus, atoms diffuse one by one, and except for the island which loses an atom, no other evolution of the island assembly is taken into account during atomic diffusion. This reasoning relies on the assumption that at each step, particles have their equilibrium shape and that the evolution of the island assembly during the diffusion of an adatom is negligible. In particular, we neglect the fact that two adatoms could meet and form a new island. This assumption is valid if the energy barrier for atomic detachment from 3D islands is much higher than the energy barrier for diffusion on the substrate. In the simulation, the time scale is defined only by the detachment rates from the islands, and the adatom diffusion trajectories are treated independently of this time scale.

Since the time scale is defined by the detachment rate from the islands, we do not need to compute true trajectories and diffusion times for individual adatoms, but we can compute simplified trajectories provided that the probability for an adatom leaving an island A to reattach to an island B is the same. This approach is a development, to the specific case of Ostwald ripening, of the multiscale algorithms[29,40] or first-passage-time algorithms used for macromolecule diffusion,[41] epitaxial growth,[42–44] or diffusion-limited reaction.[30]

The simplified trajectories are drawn in Fig. 1. For each particle (A) of radius R_D, we first compute the distance L_1 from the center of A up to the nearest particle (B) periphery. The probability for an adatom detached from A to reach, at the first passage, the distance L_1 before reattaching to A is uniform. It does not depend on the direction since the footprint of the particle on the substrate is a disk, and since there is no other island than A in the disk of radius L_1 centered on A.

The flux F of adatoms leaving the island and reaching L_1 at the first passage is directly proportional to this probability. F can be computed by considering the similar situation of a source at $r = R_D$ and a trap at $r = L_1$. The steady-state diffusion equation $\Delta c = 0$ for the boundary conditions $c(r = R_D) = c_{eq}(R_S)$ and $c(r = L_1) = 0$ is then easily obtained using the Fick equation in polar geometry. $c_{eq}(R_S)$ is the concentration of adatoms in equilibrium with a particle of radius of curvature R_S, given by Eq. (2).

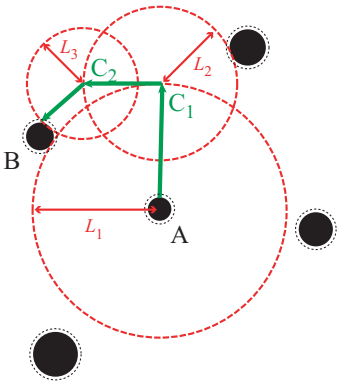

FIG. 1. (Color online) Scheme of the computation of the simplified trajectory for atomic diffusion (green arrows). An atom is evaporated from island A at a distance L_1 with a uniform probability (dotted red circles), where L_1 is the distance up to the nearest island (B). The next positions of the diffusing atom are chosen uniformly on similar circles of radius L_2,L_3,...,L_k corresponding to the distances to the nearest islands (dotted red circles). If, at any time, the atom position is within the capture area of an island (dotted black circles), the atom condenses on the island.

The solution of the equation of diffusion is

$$c(r) = c_{eq}(R_S)\frac{\ln(r/L_1)}{\ln(R_D/L_1)}. \tag{14}$$

The adatom flux reaching L_1 is thus

$$F(R_D, L_1) = 2\pi c_{eq}(R_S)D/\ln(L_1/R_D), \tag{15}$$

where D is the diffusion coefficient. Note that the boundary condition $c(r = L_1) = 0$ involved above is only used for computing the value of $F(L_1)$ and does not reflect the adatom concentration during the simulation. Eq. (15) applies for every distance L that verifies $R_D + a_S < L < L_1$, where a_S is the lattice spacing of the substrate. For $L > L_1$, the other islands act as real traps that have to be taken into account. For $L = R_D + a_S$, we find that the flux of adatoms that detach from the islands is $F(R_D, R_D + a_S) \approx 2\pi c_{eq}(R_S)DR_D/a_S$.

The diffusion coefficient D can be written as $D = \nu_d a_S^2 \exp(-E_d/kT)$, where E_d is the energy barrier for diffusion and ν_d is the attempt frequency for diffusion. Moreover, the equilibrium concentration of adatoms at the vicinity of a particle of infinite radius is given by $c_{eq}(\infty) = (\nu_e/\nu_d)(1/a_S a_P)\exp[(E_c - E_a)/kT]$, where E_c is the cohesive energy of the particle, E_a is the adsorption energy of adatoms on the substrate, a_P is the interatomic distance for atoms at the perimeter of the particle, and ν_e is the attempt frequency for detachment.

In the present KMC algorithm, the probability of reaching distance L_1 is integrated in the rate of detachment, and the event considered is the detachment from an island and

diffusion up to distance L_1, with a corresponding frequency

$$F(R_D,L_1) = 2\pi \nu_e \frac{a_s}{a_p} \exp\left(\frac{E_c - E_a + 2\gamma\Omega/R_s - E_d}{kT}\right) \times \Big/ \ln\left(\frac{L_1}{R_D}\right). \quad (16)$$

For $L = R_D + a_S$, writing $N_p = 2\pi R_D/a_p$, the number of atoms at the island periphery, we find that $F(R_D, R_D + a_S) = \nu_e N_p \exp[(E_c - E_a + 2\gamma\Omega/R_s - E_d)/kT]$ is the adatom detachment rate from the island since $\nu_e \exp[(E_c - E_a + 2\gamma\Omega/R_s - E_d)/kT]$ is the probability of detachment from an individual atomic site of the island periphery. In the simulation, the time step is the inverse of the sum of the frequencies of all possible events: $\Delta t = 1/\sum_{\text{particles}} F(R_D,L_1)$.

Once an event is selected, for example, detachment from island A, the adatom simplified trajectory is computed. A first adatom position C_1 is randomly drawn on the circle of radius L_1. The following positions, C_2,C_3, . . .,C_k are successively randomly drawn on the circles of radius L_2,L_3, . . .,L_k centered on C_1,C_2, . . .,C_{k-1}. The radius L_k of the kth circle corresponds to the distance from C_{k-1} up to the nearest island. Since there is no island in the disk of radius L_k centered on C_{k-1}, the probability of adatom diffusion from C_{k-1} up to a distance L_k is equal to unity and uniformly distributed on the circle.

Thus, adatoms diffuse by long jumps in random directions. As soon as the distance to an island is less than d_{capt}, the atom attaches to the island (see Fig. 1). In the following, we have chosen $d_{\text{capt}} = a_S$. After each detachment/attachment, the values of R_S and L_1 that could have varied are recomputed. Moreover, as soon as the distance between two islands is less than d_{capt}, i.e., when $L_1 - R_D < d_{\text{capt}}$, these islands coalesce and form a new island located at the center of mass of the two islands. This ensures that any logarithmic divergence of Eq. (16) is avoided.

IV. SIMULATION RESULTS

We have performed numerical simulations of the Ostwald ripening of hemispherical particles on a flat surface. We have chosen the case of an adsorbate/substrate couple corresponding to a very low adatom diffusion barrier and high activation energy for adatom detachment, in order to be in a coarsening regime where the adatom concentration is negligible. The parameters for the simulations have thus been set to reproduce the coarsening of Co islands on graphite, by using experimental values of the cohesive energy[45] and surface energy of cobalt,[46] and the computed value of the adsorption energy of Co on graphene.[47] For diffusion, we have used a usual attempt frequency and a low energy barrier of the same order of magnitude as the one found for Au on graphite.[48] The corresponding set of parameters is $\nu_e = 5 \times 10^{12}$ Hz, $E_c = -4.386$ eV, $E_a = -1.3$ eV, $E_d = 0.1$ eV, $\gamma = 2.5$ J m^{-2}, $\theta = \pi/2$, $a_s = 0.246$ nm, and $T = 1200$ K. Of course, using a scaling law for the time scale, the results can be easily transposed to other adsorbate/substrate couples.

Series of simulations were performed on square cells, with corresponding sizes ranging from 0.25×0.25 μm^2 up to 14.4×14.4 μm^2. Different Co coverages were simulated, equivalent to a mean film thickness ranging from 0.01 up to 1 nm. No noticeable influence of the size of the simulation cell was observed on the evolution of the island density with time until the number of islands in the box remains higher than around 20. The initial island configurations were obtained using a classical on-lattice KMC algorithm[49] adapted for 3D island nucleation through a mean-field treatment of the island morphology.

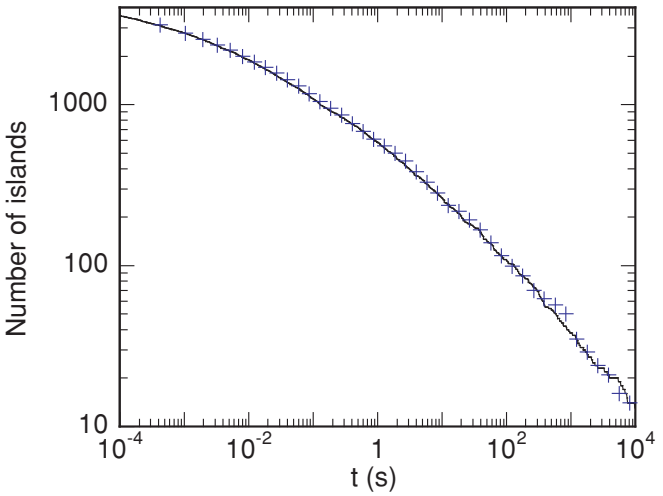

FIG. 2. (Color online) Annealing at $T = 1200$ K of 0.01 nm Co on graphite. Number of islands on a 0.25×0.25 μm^2 surface. Comparison between the results of an on-lattice classical KMC algorithm with atomic jumps between adjacent sites (blue crosses) and the results of the present off-lattice coarse-grained KMC algorithm (continuous line).

We have first compared the results of our algorithm with the results of the classical on-lattice KMC algorithm. For this purpose, the evolution of an initial configuration of 5 100 islands on a 0.25×0.25 μm^2 cell, corresponding to a mean thickness of 0.01 nm has been simulated by both algorithms. The evolution with time of the number of islands is shown in Fig. 2 for both algorithms. The results are very similar. However, simulation speed is considerably increased with our algorithm: the CPU time evolves as $t^{0.2}$, whereas for the classical KMC algorithm, the CPU time evolves as $t^{0.4}$ at the very beginning of the simulation, and as $t^{0.8}$ at the later stage. Performing a simulation is about 40 times more rapid with our algorithm than with the classical on-lattice algorithm for a simulation up to $t = 1000$ s, and about 1000 times more rapid for a simulation up to $t = 10^6$ s. Using our algorithm, it is possible to simulate the coarsening of an initially very large number of islands—for example, more than 10^6—on a large surface area, up to the final state, i.e., a unique island.

Island configurations at $t = 10^2$ s and $t = 5.6 \times 10^6$ s for coverage of 0.01 nm are presented in Figs. 3(a) and 3(b). For the whole set of simulations, we have computed the growth rate of individual particles $\partial N/\partial t$ and mean growth rate $\langle \partial N/\partial t \rangle (R_D,t)$. Since islands are hemispherical, $\partial N/\partial t = 2\pi R_D^2 dR_D/dt$. For this purpose, the growth rates of individual particles are first computed during very short time periods and the distribution obtained is further integrated over a longer time in order to reduce the data dispersion. This procedure ensures that sufficient statistics is obtained for particles of

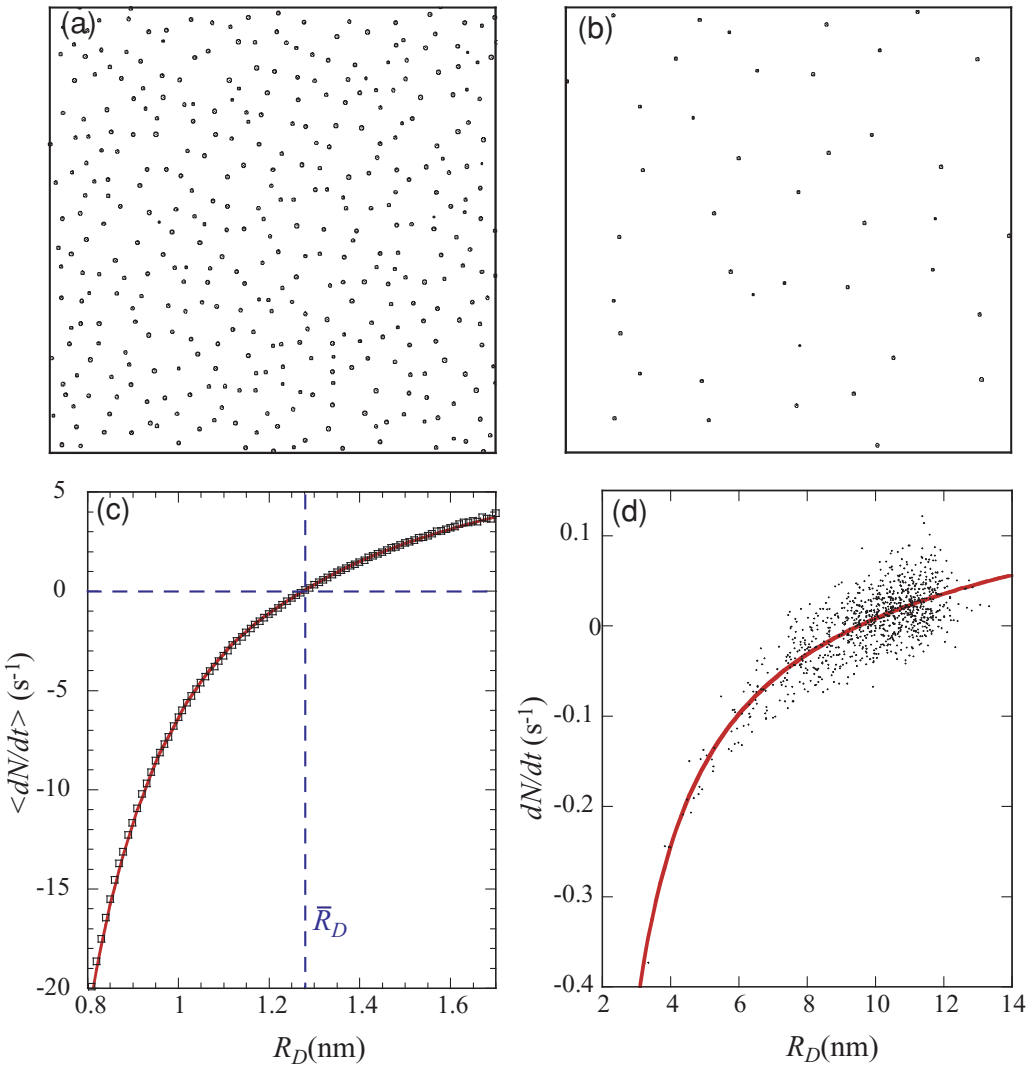

FIG. 3. (Color online) Annealing at $T = 1200$ K of 0.01 nm Co on graphite. (a) KMC configuration obtained at $t = 100$ s. 0.2×0.2 μm^2 detailed view (full size 1×1 μm^2). (b) KMC configuration obtained at $t = 5.6 \times 10^6$ s. 3×3 μm^2 detailed view (full size 14.4×14.4 μm^2). (c) Evolution of the mean growth rate $\langle \partial N/\partial t \rangle$ at $t = 100$ s. (d) Evolution of the growth rate $\partial N/\partial t$ for each particle at $t = 5.6 \times 10^6$ s. For (c) and (d), black symbols correspond to KMC results, and the red curve corresponds to $dN/dt = 2\pi\Omega R_D^2 dR_D/dt$ with dR_D/dt given by Eq. (11). The parameters for the fits are $\bar{R}_D = 1.28$ nm and $\xi = 17$ nm at $t = 100$ s and $\bar{R}_D = 9.51$ nm and $\xi = 420$ nm at $t = 5.6 \times 10^6$ s.

large size, without too much uncertainty on the growth rate of small islands, which highly depends on the particle size. The values obtained are then fitted with Eq. (12), using a least-squares-fitting procedure without taking into account the growth rate of the smallest islands representing 10 % of the size distribution.

Figure 3(d) shows the growth rate $\partial N/\partial t$ of each particle of the simulation for $t = 5.6 \times 10^6$ s [a corresponding detailed view is shown in Fig. 3(a)]. The curve is a fit using Eq. (11). Good agreement is obtained with $\bar{R}_D = 9.51$ nm and $\xi = 423$ nm, which shows that the mean-field analytical description works correctly: for this configuration, the determination of ξ using Eq. (12) indicates that $\xi = 359$ nm. However, the simulation shows a relatively large dispersion of the growth rate for different islands of same radius: for a given island, $\partial N/\partial t$ depends on the size distribution of the few nearest neighbors and not on the size distribution of the whole sample. The root-mean-square (rms) deviation of the growth rates is roughly equal to half the rms growth rate. The dispersion is higher for large islands. Figure 3(c) shows the mean growth rate $\langle \partial N/\partial t \rangle$ obtained from all configurations. Even for small island sizes, $\langle \partial N/\partial t \rangle$ is very well approximated with Eq. (11), which allows us to derive values of $\bar{R}_D$ and ξ with good precision. The comparison between the mean growth rate given by Eq. (11) and the growth rate of each island shows that the absolute value of the growth rate increases for small values of $L_1/\bar{R}_D$ and decreases for large values of $L_1/\bar{R}_D$. In the first case, two islands that are close to each other rapidly exchange atoms, and the larger one rapidly grows at the expense of the smaller one. In the second case, islands are isolated and evolve very slowly. In addition to $\bar{R}_D$ and ξ, we have followed the evolution of the island density $n_T = \int_0^\infty n(R_D) dR_D$ and of the fraction of the surface covered by the islands, φ. We find that, except at the very beginning of the simulation (for

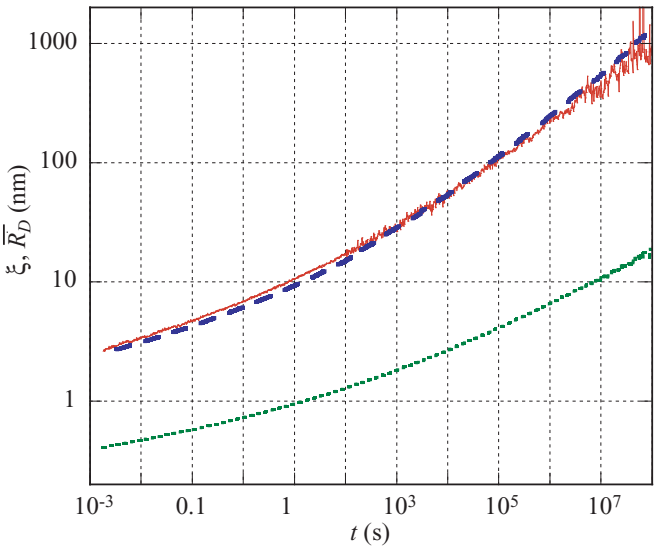

FIG. 4. (Color online) Annealing at $T = 1200$ K of 0.01 nm Co on graphite. Evolution, as a function of the time, of the screening length ξ, and of the equilibrium radius $\bar{R}_D$ determined from the KMC simulations, using a fit of the growth rate with Eq. (11). Green dotted line: $\bar{R}_D$. Red continuous line: ξ. The blue dashed line corresponds to the value of ξ determined from the KMC configurations and Eq. (12).

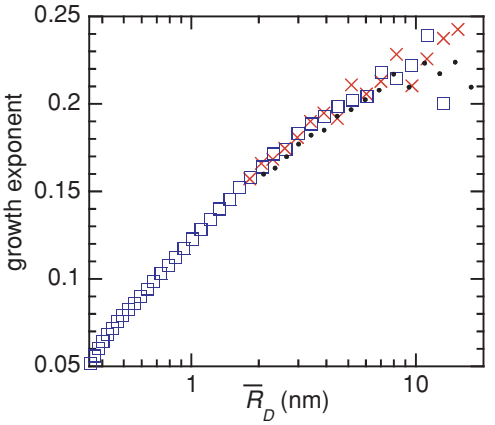

FIG. 5. (Color online) Evolution, with equilibrium radius $\bar{R}_D$, of the coarsening exponent during annealing at $T = 1200$K of Co islands on graphite. Red crosses: 0.001 nm equivalent thickness; blue squares: 0.01 nm equivalent thickness; black dots: 0.1 nm equivalent thickness.

$t < 10^{-3}$s), φ evolves as $n_T^{1/3}$ and $\bar{R}_D$ evolves as $n_T^{-1/3}$. Such exponents are easily derived if the island size distribution follows a uniform scaling behavior.

Figure 4 shows the evolution, with time, of the equilibrium radius $\bar{R}_D$ and the screening length ξ determined from the fit of $\langle \partial N/\partial t \rangle$. $\bar{R}_D$ increases slowly with time. In the limit of a very large time, the rate exponent of $\bar{R}_D(t)$, which is given by $\partial \ln(\bar{R}_D)/\partial \ln(t)$, is of the order of 0.22. This is in relative good agreement with the prediction of a 1/4 exponent for the time dependence of $\bar{R}_D$. However, this 1/4 exponent is only obtained at the end of the simulation, for $t > 10^7$s, in the limit of a very small island density covering a fraction $\varphi = 10^{-3}$ of the surface. For shorter simulation times, $\bar{R}_D$ increases at a much slower rate. Note that except at the very beginning of the simulation (for $t < 10^{-3}$s), the island density is exactly inversely proportional with the cube of the equilibrium radius.

The values of the screening length determined through Eq. (12) using the particle size distribution at each time are also drawn in the figure. Very good agreement is found in the whole range of points, indicating that the mean-field description of the Ostwald ripening process works correctly. From this self-consistent determination, we have found that ξ behaves as $\bar{R}_D^{5/3}$. Note that the mean distance between islands varies as $n_T^{-1/2}$, and thus, as $\bar{R}_D^{3/2}$. ξ increases more rapidly than the distance between islands during coarsening. For low R_D/ξ ratios, at the end of the coarsening process, more islands contribute to the screening of the diffusion from a given island, and the mean-field model should be better adapted. It should also be better adapted for low values of φ.

Figure 5 represents the evolution of the coarsening exponent, $\partial \ln(\bar{R}_D)/\partial \ln(t)$, with equilibrium radius $\bar{R}_D$ for three

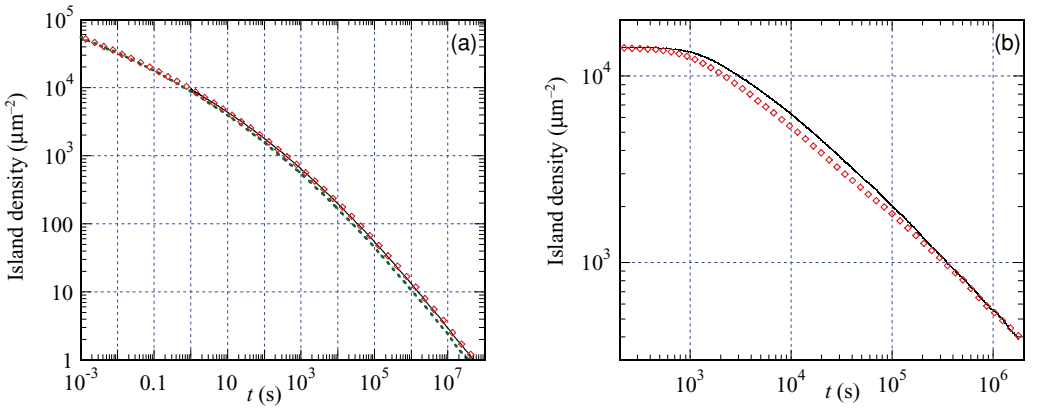

FIG. 6. (Color online) Annealing at $T = 1200$ K of an initial Co deposit on graphite. (a) Equivalent thickness: 0.01 nm. (b) Equivalent thickness: 1 nm. Comparison between KMC simulations and MS calculations of the time evolution of the island density. Red diamonds: KMC results. Green dotted line: mean-field results, starting from the KMC configuration obtained at $t = 10^{-3}$s. Black line: mean-field results, starting from the KMC configuration obtained at $t = 100$s.

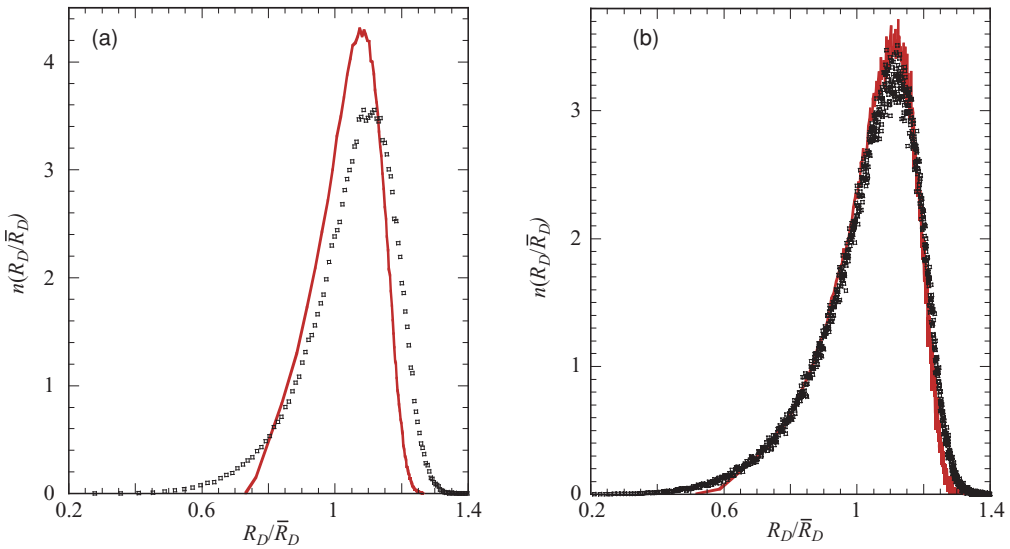

FIG. 7. (Color online) Annealing at $T = 1200$ K of 0.01 nm Co on graphite. Comparison between PSD obtained by KMC (black squares) and by numerical integration of the mean-field equations of the MS model (red curve). (a) PSD at $t = 10^2$s, starting from the KMC configuration at $t = 1$ s. (b) PSD at $t = 10^4$ s, starting from the KMC configuration at $t = 10^2$s.

different coverages: 0.1, 0.01, and 0.001 nm. The figure shows that the coarsening exponent depends mainly on the island size, at least when the fraction of the surface covered by the islands is small. Since the power-law evolution for the equilibrium radius has been derived assuming, in Eq. (2), a linear development of $c_{eq}(R_S)$ with the inverse of R_S, the $1/4$ exponent shall only be recovered when $\bar{R}_D >> 2\gamma\Omega/kT$ =3.3 nm. Of course, the coarsening exponent also depends on the precise island size distribution: if all islands have the same size, there is no coarsening since all islands have the same chemical potential.

The time evolution of the island density n_T is presented in Fig. 6. A comparison between KMC values and the analytical results of MS is presented in Figs. 6(a) and 5(b) for two coverages, namely, 0.01 nm and 1 nm. The initial configurations used for the KMC simulations are very different. For 0.01 nm, the starting configuration consists of small islands containing a few tens of atoms and covering a fraction $\varphi = 0.05$ of the surface, whereas for 1 nm, islands contain a few thousand atoms and cover half of the surface at the beginning of the simulation.

For the comparison with the MS model, we have used the KMC results at various times as input for Eqs. (11)–(13). For 0.01 nm coverage, the island density obtained by integration of the MS equations, starting from the KMC configuration obtained at $t = 10^{-3}$ s [Fig. 6(a), green dotted line], is slightly lower than the island density obtained by KMC. However, starting from the KMC configuration obtained at $t = 100$ s [Fig. 6(a), black line] gives the same density as the one obtained by KMC [Fig. 6(a), red lozenges]. For 1 nm coverage, the island density obtained by integration of the MS equations, starting from the KMC configuration obtained at $t = 100$ s [Fig. 6(b), black line], is slightly higher than the island density obtained by KMC [Fig. 6(b), red lozenges], until $t \geqslant 10^6$ s, for which both KMC and MS give similar results. For all cases, the differences between KMC and MS results for the island density do not exceed a factor of 1.25. This shows that the mean-field description of an effective medium for the diffusion is well adapted for predictions of Ostwald ripening. Two limiting cases can be identified: the first one is the small number of atoms in the islands. This is the case for 0.01 nm coverage at $t = 10^{-3}$ s, for which the mean number of atoms in the islands is of the order of 16. For such a small number of atoms, the variation of island sizes during coarsening is poorly described with a continuous model. The second limiting case is obtained when a large fraction of the surface is covered by the islands. This is the case for 1 nm coverage at $t = 100$ s, for which half of the surface is covered by the islands ($\varphi \approx 0.46$). In that case, the screening length is of the order of the island size: $\bar{R}_D/\xi \approx 1$. Good agreement between KMC and MS calculations is, however, recovered at $t = 10^6$ s, for which $\bar{R}_D/\xi \approx 0.5$ and $\varphi \approx 0.15$.

Thus, concerning the evolution of island density during coarsening, very good agreement is obtained between KMC simulations and MS integration, except for the extreme case of large values of φ and a very small mean island size.

Figure 7 presents the comparison between the particle size distributions (PSD) obtained from the KMC simulations and from the MS model. For the mean-field results, the PSD obtained from the KMC at various times have been used as input for the integration. Starting from PSD obtained at $t = 100$ s, good agreement is obtained at $t = 10^4$ s, even if the upper tail of the distribution obtained from the MS model is slightly sharper than for KMC results. Moreover, the PSD obtained is in good agreement with the theoretical stationary PSD derived by Chakraverty, using a simplified model for diffusion.[4] However, for short time inputs ($t = 1$ s), the MS model fails to correctly reproduce the PSD obtained at later times. This reflects the fact that the discrete nature of the size distribution, particularly relevant for small island sizes, cannot be correctly described by the continuous mean-field approximation. This result confirms the observations

already made concerning the time evolution of the island density.

V. CONCLUSION

The comparison between the KMC and MS results shows that our Monte Carlo algorithm is well adapted for the study of Oswald ripening, and that the mean-field description of the MS model is already accurate, except when the mean size of the islands is very small or for a large fraction of the surface, covered by the islands. For studying the time dependence of the island density, a KMC algorithm is not necessary and integration of the equations of the MS model already give correct results. Both models show that the equilibrium radius follows a power-law evolution with an exponent close to 1/4, in the limit of a very dilute system. At the beginning of coarsening, the increase of R_D is much slower.

Differences are observed for island size distribution. KMC results display size distributions wider than MS integration results. This is due to the fact that the mean-field description does not account for local variations of the size distributions.

More information can also be extracted from the KMC results, such as spatial configurations, growth rate dispersion, and dependence of the growth rate on the local island size distribution. The KMC simulations could also be used in the case of Ostwald ripening of multicomponent systems, such as metal alloys[14], for Ostwald ripening with an extra barrier for attachment. The ultrafast algorithm developed here thus opens the way to studies of more complex situations for which no analytical model of the kinetics has been developed, and for which classical algorithms are much too slow.

[1] M. Zinke-Allmang, Thin Solid Films **346**, 1 (1999).
[2] I. M. Lifshitz and V. V Slyozov, J. Phys. Chem. Solids **19**, 35 (1961).
[3] C. Wagner, Z. Electrochem. **65**, 581 (1961).
[4] B. K. Chakraverty, J. Phys. Chem. Solids **28**, 2401 (1967).
[5] M. Zinke-Allmang and L. C. Feldman, Appl. Surf. Sci. **52**, 357 (1991).
[6] M. Zinke-Allmang, Nucl. Instrum. Methods Phys. Res. B **64**, 113 (1992).
[7] J. G. McCarty, G. Malukhin, D. M. Poojary, A. K. Datye, and Q. Xu, J. Phys. Chem. B **109**, 2387 (2005).
[8] M. O. Blunt, C. P. Martin, M. Ahola-Tuomi, E. Pauliac-Vaujour, P. Sharp, P. Nativo, M. Brust, and P. J. Moriarty, Nature Technol. **2**, 167 (2007).
[9] P. Wynblatt and N. A. Gjostein, Acta Metall. **24**, 1165 (1976).
[10] G. S. Rohrer, C. L. Rohrer, and W. W. Mullins, J. Am. Ceram. Soc. **85**, 675 (2002).
[11] C. V. Thompson, Acta. Metall. **36**, 2929 (1988).
[12] G. P. Zhang, M. Hupalo, M. Li, C. Z. Wang, J. W. Evans, M. C. Tringides, and K. M. Ho, Phys. Rev. B **82**, 165414 (2010).
[13] J.-N. Aqua, T. Frisch, and A. Verga, Phys. Rev. B **76**, 165319 (2007).
[14] D. Alloyeau, G. Prévot, Y. Le Bouar, T. Oikawa, C. Langlois, A. Loiseau, and C. Ricolleau, Phys. Rev. Lett. **105**, 255901 (2010).
[15] J. A. Marqusee, J. Chem. Phys. **81**, 976 (1984).
[16] G. Nandipati, Y. Shim, J. G. Amar, A. Karim, A. Kara, T. S. Rahman, and O. Trushin, J. Phys. Condens. Matter **21**, 084214 (2009).
[17] V. M. Kaganer, W. Braun, and K. K. Sabelfeld, Phys. Rev. B **76**, 075415 (2007).
[18] K. Shorlin, S. Krylov, and M. Zinle-Allmang, Physica A **261**, 248 (1998).
[19] J. Viñals and W. W. Mullins, J. Appl. Phys. **83**, 621 (1998).
[20] M. S. Levine, A. A. Golovin, S. H. Davis, and P. W. Voorhees, Phys. Rev. B **75**, 205312 (2007).
[21] J. A. Floro, M. B. Sinclair, E. Chason, L. B. Freund, R. D. Twesten, R. Q. Hwang, and G. A. Lucadamo, Phys. Rev. Lett. **84**, 701 (2000).
[22] J. G. Amar and F. Family, Phys. Rev. B **54**, 14742 (1996).
[23] A. V. Zverev, K.Yu. Zinchenko, N. L. Shwartz, and Z. Sh. Yanovitskaya, Nanotech. Russia **4**, 215 (2009).
[24] C.-L. Li and C.-K. Hu, Appl. Phys. Lett. **96**, 093101 (2010).
[25] M. T. Lung, C.-H. Lam, and L. M. Sander, Phys. Rev. Lett. **95**, 086102 (2005).
[26] G. Sitja, R. Omar Uñac, and C. R. Henry, Surf. Sci. **604**, 404 (2010).
[27] Y. A. Kryukov and J. G. Amar, Phys. Rev. B **81**, 165435 (2010).
[28] R. A. Bennett, D. M. Tarr, and P. A. Mulheran, J. Phys.: Condens. Matter **15**, S3139 (2003).
[29] M. A. Novotny, Phys. Rev. Lett. **74**, 1 (1995).
[30] T. Opplestrup, V. V. Bulatov, G. H. Gilmer, M. H. Kalos, and B. Sadigh, Phys. Rev. Lett. **97**, 230602 (2006).
[31] R. D. Gretz, J. Chem. Phys. **45**, 3160 (1966).
[32] B. J. Block, S. K. Das, M. Oettel, P. Virnau, and K. Binder, J. Chem. Phys. **133**, 154702 (2010).
[33] A. Bortz, M. Kalos, and J. Lebowitz, J. Comput. Phys. **17**, 10 (1975).
[34] O. Trushin, A. Karim, A. Kara, and T. S. Rahman, Phys. Rev. B **72**, 115401 (2005).
[35] A. Karim, A. N. Al-Rawi, A. Kara, T. S. Rahman, O. Trushin, and T. Ala-Nissila, Phys. Rev. B **73**, 165411 (2006).
[36] R. C. Tolman, J. Chem. Phys. **16**, 758 (1948).
[37] B. J. Block, S. K. Das, M. Oettel, P. Virnau, and K. Binder, J. Chem. Phys. **133**, 154702 (2010).
[38] C. T. Campbell, S. C. Parker, and D. E. Starr, Science **298**, 811.
[39] J. Goniakowski and C. Mottet, Phys. Rev. B **81**, 155443 (2010).
[40] J. P. DeVita, L. M. Sander, and P. Smereka, Phys. Rev. B **72**, 205421 (2005).
[41] J. A. Given, J. B. Hubbard, and J. F. Douglas, J. Chem. Phys. **106**, 3761 (1997).
[42] C. C. Chou and M. L. Falk, J. Comput. Phys. **217**, 519 (2006).
[43] V. I. Tokar and H. Dreyssé, Phys. Rev. E **77**, 066705 (2008).
[44] V. I. Tokar and H. Dreyssé, Phys. Rev. B **80**, 161403(R) (2009).
[45] D. R. Lide, *CRC Handbook of Chemistry and Physics*, 79th ed. (CRC, Boca Raton, FL, 1998), p. 5.13.
[46] W. R. Tyson and W. A. Miller, Surf. Sci. **62**, 267 (1977).
[47] Y. Mao, J. Yuan, and J. Zhong, J. Phys.: Condens. Matter **20**, 115209 (2008).
[48] P. Jensen, X. Blase, and P. Ordejón, Surf. Sci. **564**, 173 (2004).
[49] G. Prévot, H. Guesmi, and B. Croset, Surf. Sci. **601**, 2017 (2007).